ELSEVIER

Journal of Electron Spectroscopy and Related Phenomena 123 (2002) 303–314

JOURNAL OF ELECTRON SPECTROSCOPY and Related Phenomena

www.elsevier.com/locate/elspec

Generalized oscillator strengths for C 1s excitation of acetylene and ethylene

A.P. Hitchcock[a,*], S. Johnston[a], T. Tyliszczak[a], C.C. Turci[b], M. Barbatti[b], A.B. Rocha[b], C.E. Bielschowsky[b]

[a]*Department of Chemistry, McMaster University, Hamilton, Ont., Canada L8S 4M1*
[b]*Instituto de Química, Universidade Federal do Rio de Janeiro, Rio de Janeiro, 21910-900, RJ, Brazil*

Received 2 December 2001; received in revised form 8 January 2002; accepted 23 January 2002

Dedicated to Professor C.E. Brion on the occasion of his 65th birthday

Abstract

The generalized oscillator strength profiles for discrete C 1s excited states of C_2H_2 and C_2H_4 have been derived from angle-dependent inelastic electron scattering cross-sections measured with 1300 eV final electron energy. The measured GOS profiles for the strong C 1s→π* transition in each species are compared to theoretical calculations computed within the first Born approximation, using ab-initio generalized multi structural wave functions. These wave functions include relaxation, correlation and hole localization effects. Theory predicts large quadrupole contributions to the π* GOS of each species, analogous to those previously reported for computed GOS profiles for O 1s→π* excitation of CO_2. We find good agreement between experiment and theory as to the shape of the π* GOS but, when the relative GOS extracted from the experimental data is normalized to the optical oscillator strength at $K^2=0$, the magnitude is in better agreement with the GOS computed for only the dipole channel than for the sum of the dipole and quadrupole channels. © 2002 Elsevier Science B.V. All rights reserved.

Keywords: Generalized oscillator strength; Electron scattering; EELS; Quadrupole transitions

1. Introduction

The career of Chris Brion has been characterized by a systematic development of novel instrumentation and advanced techniques for measurement of cross-sections of electronic processes and their use in the elucidation of atomic and molecular structure. Early studies dealt with measurements of electron impact ionization thresholds, threshold electron energy loss spectroscopy using a novel SF_6 scavenger technique, and variable impact energy and variable scattering angle valence shell electron energy loss spectroscopy (VSEELS). These results are summarized in an early review, which also nicely summarizes the status of experimental electron spectroscopy in ~1970 [1]. In the 1970s, a branch of Brion's work developed which focused on inner shell electron energy spectroscopy of molecules in the dipole regime. The work reported in this paper is a continuation of the pioneering work of the Brion

*Corresponding author. Tel.: +1-905-525-9140x24749; fax: +1-905-521-2773.
E-mail address: aph@mcmaster.ca (A.P. Hitchcock).

0368-2048/02/$ – see front matter © 2002 Elsevier Science B.V. All rights reserved.
PII: S0368-2048(02)00029-4

group on angle-dependent cross-sections for dipole and non-dipole valence shell excitation [2–8] and dipole inner-shell spectroscopy [9–12].

The study of absolute generalized oscillator strength profiles (GOS), also known as Bethe surfaces, provides a means of improving our understanding of many high energy phenomena which are important in fields ranging from atmospheric chemistry to radiation physics. To date, despite the wide range of applications, experimental exploration of these absolute generalized oscillator strength cross-sections has remained relatively limited, particularly for inner shell processes. This work is part of a systematic combined experimental and computational study whose goal is to build a database of GOS profiles for the inner shell excited and ionized states of molecules. We hope that comparison among related molecules will give insight into the relationship among molecular structure, bonding and GOS profile.

Previous work from our group in this area includes the study of dipole and non-dipole spectroscopy and GOS profiles for a number of molecules. Using high energy resolution, the (C $1s^{-1}$, π^*) triplet state spectroscopy of carbon monoxide, benzene, ethylene and acetylene has been investigated using electron energy loss spectroscopy with low-energy (near-threshold) excitation [13]. The momentum transfer dependence of the spin forbidden excitation to the (C $1s^{-1}$, π^*) $^3\Pi$ state of carbon monoxide has been measured and compared to theoretical calculations which included excited state potential curves and vibrational fine structure [14]. The core excitation spectroscopy of SF_6 has been studied intensively by many groups because it is a model for species in which a central atom is surrounded by a 'cage' of electronegative atoms. Notwithstanding the extensive earlier work, systematic investigation of the S 2p, S 2s and F 1s electron energy loss spectra of SF_6 in the non-dipole scattering regime [15–17] revealed several, previously unknown, S 2p non-dipole transitions around 181 eV, which at momentum transfers (K) greater than K^2=40 a.u.$^{-2}$ become the dominant S 2p spectral feature [17]. Generalized oscillator strength (GOS) profiles for discrete and continuum S 2p excitations of SF_6 have been derived over a wide momentum transfer range (1 a.u.$^{-2}$<K^2<40 a.u.$^{-2}$) [18,19]. In addition to SF_6, the generalized oscillator strength profiles for C 1s and O 1s excitations in CO_2 [20,21] were derived over (2 a.u.$^{-2}$<K^2<70 a.u.$^{-2}$), and interpreted with the aid of high level ab initio calculations. A review of inner-shell electron spectroscopy and GOS profile measurements of gas phase molecules has been published recently [22].

Electron energy loss spectroscopy (EELS) can provide absolute oscillator strength cross-sectional information [1,23,24]. In the regime where the first Born approximation applies, Bethe has shown that the inelastic electron scattering process can be described by a generalized oscillator strength (GOS, df/dE) [25,26] which is defined as:

$$df/dE = (E_n/2K^2).|\langle F|e^{ik.r}|I\rangle|^2 = (E_n k_o K^2/k_1).(d^2\sigma/d\Omega\, dE) \quad (1)$$

where E_n is the energy loss, $\langle F|e^{ik.r}|I\rangle$ is the transition matrix for coupling the initial ($|I\rangle$) and final ($|F\rangle$) states of the transition, K is the magnitude of the momentum transfer vector, k_o is the momentum of the incident electron of energy E_o, k_1 is the momentum of the inelastically scattered electron of energy $E_1 = E_o - E_n$, and $d^2\sigma/d\Omega\, dE$ is the differential cross-section for inelastic scattering into a solid angle $d\Omega$ over the energy loss range dE. The GOS (df/dE) expresses the transition intensity as a function of momentum transfer per unit angle and unit energy. The GOS conveniently separates the target aspects of the intensity ($\langle F|e^{ik.r}|I\rangle$) and kinematic factors ($E_n/2K^2$) which are dictated by the experimental conditions (E_0 and θ). In the Bethe–Born treatment [23,26], the generalized oscillator strength is related to a power series expansion in K^2 with expansion coefficients related to electric multipole matrix elements:

$$df/dE = A + BK^2 + CK^4 + \cdots \quad (2)$$

where $A = \langle\varepsilon_1\rangle^2$ (proportional to the optical oscillator strength), $B = (\langle\varepsilon_2\rangle^2 - 2\varepsilon_1\varepsilon_3)$, $C = (\langle\varepsilon_3\rangle^2 - 2\varepsilon_2\varepsilon_4 + 2\varepsilon_1\varepsilon_5)$ and, ε_i is the ith order electric multipole matrix element.

Generalized oscillator strength profiles can be generated by systematically varying momentum transfer, typically by scanning the scattering angle, and measuring the energy loss intensity. After suitable corrections and normalization to optical oscillator strengths [19,20] this yields the GOS profile, or

the absolute GOS as a function of momentum transfer for a given energy loss (transition).

This paper reports experimental GOS profiles for several discrete C 1s excitations of ethylene and acetylene, along with comparison to calculated GOS profiles for the C 1s→π* transitions. The dipole regime inner shell energy loss [10,12,27,28] and photoabsorption spectra [29–32] of these species have been reported and interpreted in considerable detail. Theoretical calculations of the π* optical oscillator strengths have been reported for acetylene [33–35] and ethylene [33]. Prior to this study, only the GOS profile for the C 1s→π* transition of acetylene [35] has been measured and compared to the GOS computed for the C1s→π* transition [35]. In that work, the experimental GOS values were normalized to the theoretical result at a low K value, and thus that study did not provide an independent evaluation of the absolute GOS for the C1s→π*. For this investigation, the inelastic scattering spectra were recorded using McVAHRES, the McMaster Variable Angle, High Resolution, Electron Spectrometer. This instrument, its operation, and the procedures for data analysis, have all been described in detail previously [19,20]. This work is the first report of data collected with a new position sensitive parallel detection system [36] which has greatly increased data collection rates for the weak large scattering angle signals. A brief description of this detector was presented earlier [22].

Through this study, we seek to characterize the GOS profiles and determine if their magnitude and shape can provide a way to differentiate and thus help identify core excited states. Comparison to theoretical predictions of absolute generalized oscillator strengths is also an important motivation for this work. Ethylene and acetylene each contain chemically equivalent carbon atoms and an inversion symmetry element. The momentum transfer dependence of the relative intensities of the dipole allowed $1s\sigma_u \rightarrow \pi_g^*$ and dipole forbidden, quadrupole allowed $1s\sigma_g \rightarrow \pi_g^*$ in C_2H_2 and C_2H_4 are of considerable interest. The computational part of our recent study of CO_2 [20] suggested that in CO_2, which has analogous symmetry equivalent O atoms, the O $1s\sigma_u \rightarrow \pi_u^*$ quadrupole transition turns on at quite low momentum transfer and becomes as intense as the dipole channel. This behavior is quite different from the relative strength of dipole versus quadrupole transition intensities in lower symmetry species. The theoretical component of this work has evaluated both the dipole allowed $1s\sigma_u \rightarrow \pi_g^*$ and dipole forbidden, quadrupole allowed $1s\sigma_g \rightarrow \pi_g^*$ GOS profiles.

2. Experimental

The samples were obtained commercially (acetylene—Matheson 99%; ethylene—Liquid Air 99.9%) and were used as supplied. In the configuration of the spectrometer (Fig. 1) used in this work, an unmonochromated electron beam was incident on gas in the collision region, inside a gas cell. Inelastically scattered electrons are decelerated and velocity selected by an electrostatic electron analyzer. The scattering angle is varied by rotating the analyzer relative to the fixed incident electron beam direction. The gun and analyzer input lens were carefully mechanically aligned. The measurements were made in constant final energy mode. The incident electron energy is the sum of the final electron energy (1300 eV in this case), the measured energy loss, and the analyzer pass energy (30 eV). The energy resolution was 0.9 eV fwhm.

Electron energy loss spectra were recorded over a scattering range of 1–36°, corresponding to momentum transfer values (K^2) between 1 and 40 a.u.$^{-2}$. Data points above $K^2 = 34$ a.u.$^{-2}$ were not reliable and have been excluded from this presentation. The signal level from gas outside the gas cell was measured by introducing the same pressure of gas from a separate inlet. This signal was found to be negligible because of the more than ~30-fold higher concentration of gas in the cell relative to regions outside the cell. The no-sample background signal (from electron scattering from surfaces, and electronic noise) was featureless and always less than 2% of the signal even at large scattering angle so no corrections have been made. Measurements of the angular dependence of the He valence energy loss spectrum were used to establish the absolute scattering angle scale and to determine a geometrical correction factor, which accounts for the variation with scattering angle in the volume of the intersec-

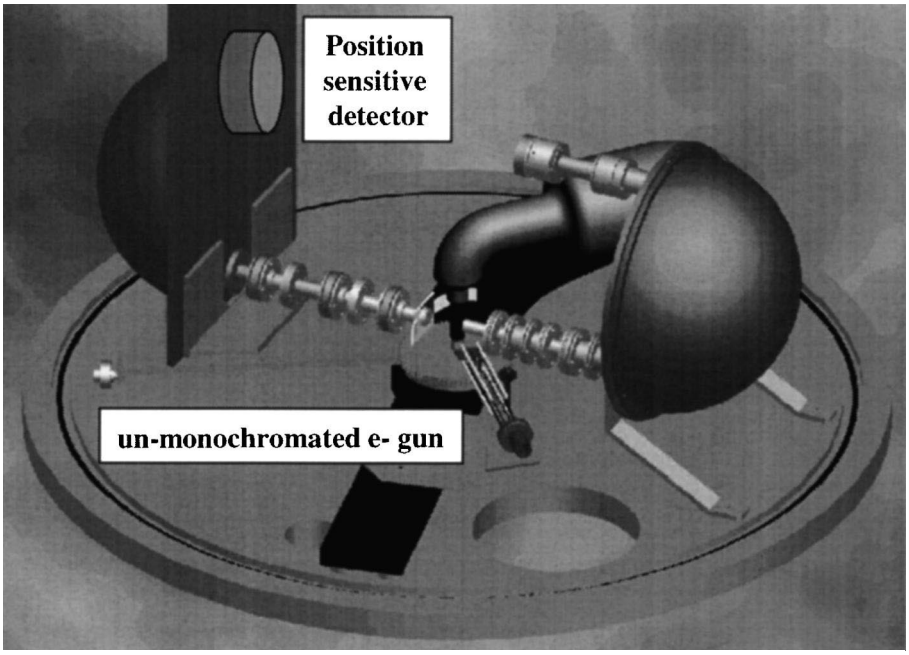

Fig. 1. McMaster variable angle high resolution electron spectrometer (McVAHRES) apparatus. The parallel detector was newly installed for this work.

tion of sample gas, incident electron beam and analyzer viewing cone. With effusive jets we have found that the large variation in the scattering path length as a function of scattering angle must be corrected in order to obtain meaningful results [18,20,37]. However, with the gas cell, the variation in scattering path is much smaller. The geometric correction factor, evaluated by comparing the GOS curve for He 2s and 2p valence states to literature values, was very minor and thus no such correction was applied in this work.

The spectrum recorded at each scattering angle was corrected for variations in dwell time (which was varied to achieve approximately constant statistics), gas pressure, and beam current. The results presented for each species are based on a single pass through the measured scattering angle range (1–36°), which took 3–5 days. Repeat measurements gave similar results. The spectrum at each angle was background subtracted (linear fit to pre-C 1s signal) to isolate the C 1s excitation from the underlying valence ionization signals. At an impact energy of 1615 eV, the valence Compton scattering peak passes underneath the C 1s energy loss signal in the 10–20° scattering range. Thus we found it to be important to make a careful estimate of this background by extrapolation of a sufficiently long range of the pre-C 1s energy loss signal. In fact, the slope of the background changes sign in part of this scattering angle range. The nominal energy loss scale from the instrument was calibrated by setting the centroid of the C 1s$\rightarrow\pi^*$ transition to the literature energy [10].

The normalized spectra were fit to a model consisting of a combination of Gaussian lines and an arctangent edge jump function [19,20]. The positions, and assignments for each spectral feature are summarized in Table 1. The cited uncertainly in the peak positions reflects the imprecision of the fit, standard deviation, as well as an estimate of systematic errors and uncertainty in absolute calibration. The relative differential cross-sections were then obtained from the peak areas determined by a simultaneous constrained curve fit to the spectra at all angles. The constraints employed were to require a fixed energy for each transition at all angles, and the same width for each peak at any single angle.

Table 1
Energies and assignments for C 1s excitations of C_2H_2 and C_2H_4

Feature	Type[a]	Position (eV)	Assignment
C_2H_2			
1	G	285.7[b]	π*
2	G	287.9	3s
3	G	288.9	3p
4	G	290.0(4)	Higher Ryd
Edge	A	291.2(4)	IP
C_2H_4			
1	G	284.7[b]	π*
2	G	285.0	π* + vib.[c]
3	G	287.2	3s
4	G	287.9	3p
5	G	289.3	Higher Ryd
Edge	A	290.7(9)	

[a] G, Gaussian line; A, arctangent edge step.
[b] This value was used for energy calibration.
[c] The π* peak of ethylene is quite asymmetric due to vibrational fine structure. This was simulated by a combination of two Gaussians.

The widths varied from 0.85 to 1.0 eV, being somewhat larger at higher scattering angles on account of slow drifts in the energy scales over long sampling periods. The differential cross-sections were then converted to relative GOS curves by applying the kinematic correction factor (Eq. (1)). The absolute generalized oscillator strength scale was then set by calibrating an extrapolation to $K^2 = 0$ of the GOS profile for the intense C 1s→π* transitions and setting that extrapolated value to our best estimate of the optical oscillator strength (OOS) [29–32]. OOS values of 0.142 for C_2H_2 and 0.075 for C_2H_4 were used, as justified below. Our estimates of the uncertainty (non-systematic errors) in the GOS profile are given by plotted error bars. These were estimated through a combination of statistical analysis of error propagation through our data work-up procedures, as well as the uncertainty in our curve fits which was estimated from the scatter in several repeats of the curve fit using somewhat different assumptions about spectral content and constraints. The absolute GOS scales are somewhat more uncertain due to uncertainties in the extrapolation of the relative GOS to $K^2 = 0$. This larger uncertainty in the absolute GOS value is indicated by the oversized error bar at $K^2 = 1$ a.u.$^{-2}$ in Fig. 8.

3. Computational methods

We have calculated the Optical (OOS) and Generalized Oscillator Strength (GOS) for the excitation from the ground $X^1\Sigma_g^+$ electronic state to the $1\sigma_g$ (C 1s)→$1\pi_g$ and $1\sigma_u$ (C 1s)→$1\pi_g$ inner-shell electronic excited states of C_2H_2 and C_2H_4. The electronic wave functions for the ground ($X^1\Sigma_g^+$) and C 1s excited states were determined with the configuration-interaction (CI) method expanded on a (12s, 6p, 1d)/[10s,4p,1d] Gaussian basis set [38]. Occupied and improved virtual orbitals were determined independently for the ground state and each excited state and, as a consequence, are not orthogonal. This means that the molecular basis for the CI calculation was optimized for each molecular state and includes, for the excited states, the strong relaxation that takes place in the formation of an inner-shell excited state. Configuration-interaction calculations were carried out for each molecular state, allowing single and double excitations for the reference configuration to a virtual space composed of three virtual orbitals for each symmetry (σ_g, π_g, σ_u or π_u).

Generalized multistructural (GMS) wavefunctions

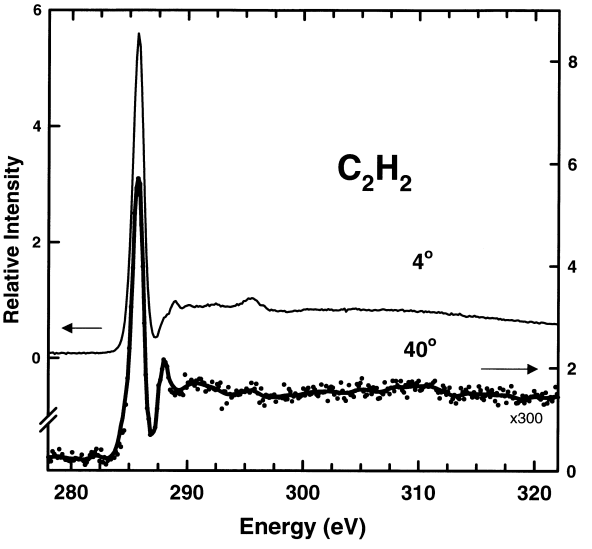

Fig. 2. Comparison of C 1s inner shell electron energy loss spectra of acetylene recorded with 1300 eV residual electron energy at 4 and 40° scattering angles. The 40° spectrum has been amplified 300 times.

[39,40] were used in order to take into account core hole localization effects without breaking the full molecular symmetry. The GMS wavefunction is defined as

$$\Psi_{\mathrm{GMS}} = \sum_{l=1}^{\mathrm{NSTRUCT}} \sum_{i=1}^{\mathrm{NSEF}} c_i^l \Phi_i^l \qquad (3)$$

where Φ_i^l represents the ith spin-adapted function of the lth bonding structure and c_i^l its weight in the expansion shown in Eq. (3) and is calculated variationally. Each Φ_i^l is a Hartree–Fock or a CI wavefunction. We have considered the following three structures ($l=3$ in Eq. (3)) for each excited state:

Structure 1 is a Hartree–Fock wave function with molecular orbitals optimized in the presence of a 1s hole localized upon the first carbon atom.

Structure 2 is a Hartree–Fock wave function with molecular orbitals optimized in the presence of a 1s hole localized upon the second carbon atom.

Structure 3 is a SD-CI wavefunction (SD = single and double) with molecular occupied and virtual orbitals optimized in the presence of a 1s delocalized hole.

This approach considers relaxation, valence corre-

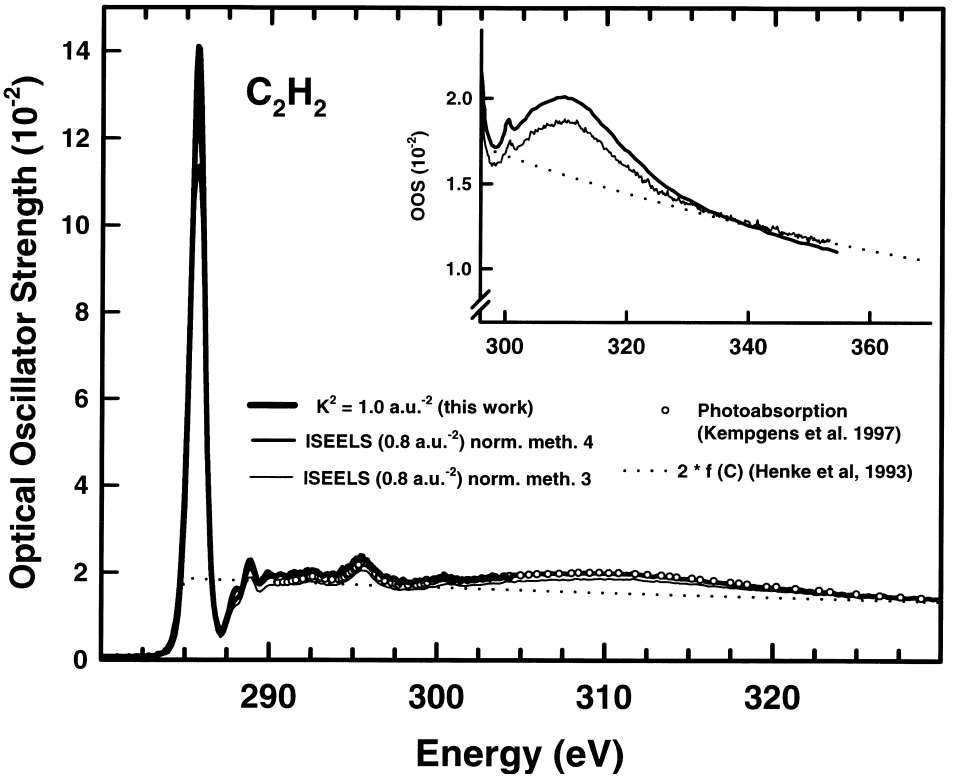

Fig. 3. C 1s component of the optical oscillator strength (OOS) spectrum of acetylene derived from ISEELS data recorded using higher impact energy (2.8 keV) and thus lower momentum transfer ($K^2=0.8$ a.u.$^{-2}$). The as-recorded energy loss spectrum was first subjected to kinematic correction (Eq. (1)). This was followed by normalization using two different techniques. In the first (labeled method 4 in the footnote to Table 2) the continuum intensity of the kinematic-corrected ISEELS spectrum was matched to the continuum OOS for C_2H_2 [32] measured using a true absorption technique [41]. In the second (labeled method 3 in the footnote to Table 2) the continuum intensity of the kinematic-corrected ISEELS spectrum was matched to twice the optical oscillator strength tabulated for atomic carbon [42]. The inset expands the comparison of these methods in the continuum. Conventional wisdom says that the experimental data should approach the atomic data asymptotically. The data from the McVAHRES measurement at lowest scattering angle (corresponding to $K^2=1.0$ a.u.$^{-2}$), matched to the normalization method 4 ISEELS result, is also plotted for comparison.

lation and localization effects and retains the full molecular symmetry [39,40]. The wave functions for the ground (CI) and excited states (CI or GMS), in spite of being a suitable description for the states involved in the transition, have the disadvantage of being mutually non-orthogonal. This requires considerable computational effort for calculating the transition matrix elements. The matrix elements for the scattering amplitude between the nonorthogonal wave functions were calculated using a bi-orthogonalization procedure [38]. For this purpose, unitary transformations are applied to the two sets of N non-orthogonal molecular orbitals, turning $(N-1)$ of them orthogonal.

4. Results

4.1. Acetylene

The carbon 1s spectra of acetylene recorded at scattering angles of 4 and 40°, respectively are shown in Fig. 2. The 4° spectrum is very similar to published ISEELS results with a comparable resolution [10,12]. The 40° spectrum shows the same transitions but the relative intensities for the features between 288 and 298 eV have changed considerably. At large scattering angles, the π* intensity decreases relative to that of the Rydberg and continuum intensities. In addition, the 3s transition (287.9 eV) increases significantly relative to the 3p transition (288.9 eV).

In order to determine reliable optical oscillator strength values for the C 1s→π* transition, we have used our dipole regime ISEELS result (recorded at $K^2 = 0.8$ a.u.$^{-2}$) [12] to extend the absolute continuum photoabsorption cross-sections of acetylene reported by Kempgens et al. [32] to the discrete region. Since those optical values were measured using a true absorption technique [41] they are likely to be the most accurate experimental values available. One of the advantages of energy loss spectroscopy is that, since it is not a resonance technique, it is not subject to distortion by absorption saturation. Thus the extrapolation procedure, which we have been obliged to use since a direct, accurate measurement of the π* OOS does not seem to have been reported as yet in the literature, may have some

Table 2
Summary of experimental[a] and theoretical estimates of the optical oscillator strengths for the C 1s→π* transitions in C_2H_2 and C_2H_4

Value	Method[b]	Normalization	Reference
C_2H_2			
Experiment			
0.146	ISEELS (E_o = 2785 eV)	1	[28]
0.12(1)	ISEELS (E_o = 2785 eV)	2	[12]
0.12(2)	ISEELS (E_o = 1800 eV)	2	[13]
0.126	ISEELS (E_o = 2785 eV)	3	This work
0.148	ISEELS (E_o = 1290 eV)[c]	–	[35]
0.142	ISEELS (E_o = 2785 eV)	4	[32]
Theory			
0.282	Small basis Hartree–Fock		[34]
0.168	Multireference doubles CI		[33]
0.175	GMS-CI		[35]
0.175	GMS-CI		This work
C_2H_4			
Experiment			
0.068	ISEELS (E_o = 2785 eV)	1	[28]
0.053	ISEELS (E_o = 2785 eV)	2	[12]
0.06(1)	ISEELS (E_o = 1800 eV)	2	[13]
0.061	ISEELS (E_o = 2785 eV)	3	This work
0.075	ISEELS (E_o = 2785 eV)	4	[32]
Theory			
0.087	Multi-reference doubles CI		[33]
0.098	GMS-CI		This work

[a] See Figs. 3 and 6. In contrast to the method described in detail in Ref. [12], we have chosen not to subtract the valence background, but rather to adjust the kinematic correction and the scaling so that there is best match to atomic values [42] outside the molecular region, to both lower and higher energies. Note the relatively large spread in the results from the three different methods used to normalize the converted ISEELS data to atomic cross-sections.

[b] Dipole regime (small momentum transfer, $K^2 = 0.8$ a.u.$^{-2}$) ISEELS spectra were converted to absolute optical oscillator strength scales by kinematic correction (Eq. (1)) followed by one of the following normalization methods.

1. Setting C 1s continuum intensity at IP + 25 eV (25 eV above the C 1s ionization potential) to the value of 0.0078 per carbon atom [28], as determined from tabulated optical oscillator strengths of Henke et al. [42].
2. Matching asymptotic C 1s continuum intensity to the tabulated optical oscillator strengths of Henke et al. [42], as described in Ref. [12].
3. Matching asymptotic pre-edge (below 282 eV) and far C 1s continuum intensity (above 320 eV) to the tabulated optical oscillator strengths of Henke et al. [42].
4. Matching continuum shape (292–350 eV) to the absolute optical values reported by Kemgens et al. [32].

[c] Value reported from ISEELS recorded at $K^2 = 1.4$ a.u.$^{-2}$ and placed on an absolute scale by matching to the theoretical GMS-CI value at $K^2 = 1.4$ a.u.$^{-2}$ [35].

advantages. Fig. 3 compares the ISEELS data converted to an optical oscillator strength scale in two different ways. In one case we have made the kinematic correction, then scaled to match the spectrum to that reported by Kempgens et al. [32] in the 292–325 eV region (in Table 2, this is called normalization method 4). In a second method, we have adjusted the kinematic correction and scaling to achieve best fit above 335 eV and below 285 eV to twice the tabulated optical oscillator strength for photoabsorption of elemental carbon [42] (in Table 2, this is called normalization method 3). This is similar to the method we have used for many years in reporting our ISEELS results [12], except that the intensity below and far above the molecular structure around the excitation onset was used, instead of a prior background subtraction to remove the underlying valence ionization continuum [12] (in Table 2, the latter procedure is called normalization method 2). The insert to Fig. 3 suggests the far-continuum shape reported by Kempgens et al. [32] has a different shape than that of the tabulated atomic oscillator strengths [42]. At first inspection, it seems unreasonable that the experimental continuum signal above 342 eV lies below the atomic value. However, the total oscillator strength per C atom (integrated from threshold to infinity) for C 1s excitation and ionization of a carbon atom in a molecule must be the same as that for an isolated carbon atom. Thus the intensity in the strong near edge resonances must be compensated by a reduced intensity relative to atomic values in other regions, as discussed elsewhere [12]. The optical oscillator strength values for

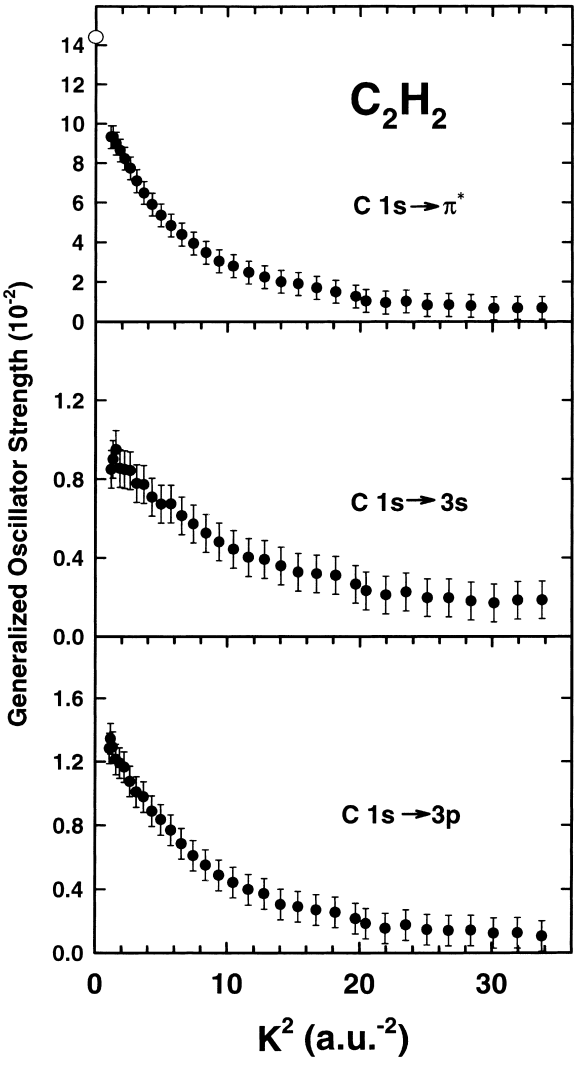

Fig. 4. Generalized oscillator strength profiles for the π*, 3s and 3p C 1s excited states of acetylene. The absolute GOS scale was established by setting the extrapolated π* GOS at $K^2 = 0$ a.u.$^{-2}$ to an optical oscillator strength of 0.142, derived as outlined in the text.

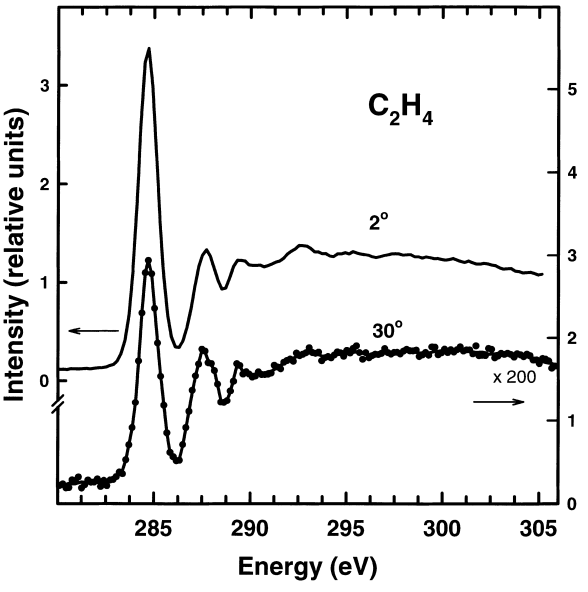

Fig. 5. C 1s inner shell electron loss spectrum of ethylene recorded with 1300 eV residual electron energy at 2 and 30° scattering angles. The 30° spectrum has been amplified 200 times.

the C 1s→π* transition of acetylene as determined by these methods are reported in Table 2 in comparison to literature computed values. We consider the OOS determined by matching to the experimental photoabsorption continuum (method 4) to be the most accurate and have used this value to derive the absolute GOS scale by extrapolation of the relative GOS curve to $K = 0$.

Fig. 4 plots the GOS profiles for the π*, 3s and 3p features. The 3s and 3p relative GOS were converted to absolute GOS by multiplication by the same scale factor used to determine the absolute GOS scale for the π* transition. There are some hints of structure in the 3s and 3p GOS profiles, but the effects are not considered statistically meaningful. The GOS profile for the 3s state is considerably less steep than those for the π* and 3p states, reflecting its relatively greater intensity at large scattering angle.

4.2. Ethylene

Carbon 1s spectra of ethylene at 2 and 30° are shown in Fig. 5. The 2° spectrum is similar to previously published dipole ISEELS results at a comparable resolution [10]. As with acetylene the high angle spectrum has similar transition features but the relative intensities have changed. In particular, the π* transition (284.7 eV) decreases intensity significantly relative to Rydberg structure and the continuum. This effect is much more pronounced in ethylene than in acetylene.

As with acetylene, in order to determine reliable optical oscillator strength values for the C 1s→π* transition, we have used our dipole regime ISEELS result (recorded at $K^2 = 0.8$ a.u.$^{-2}$) [12] to extend the absolute continuum photoabsorption cross-sections of ethylene reported by Kempgens et al. [32] to the

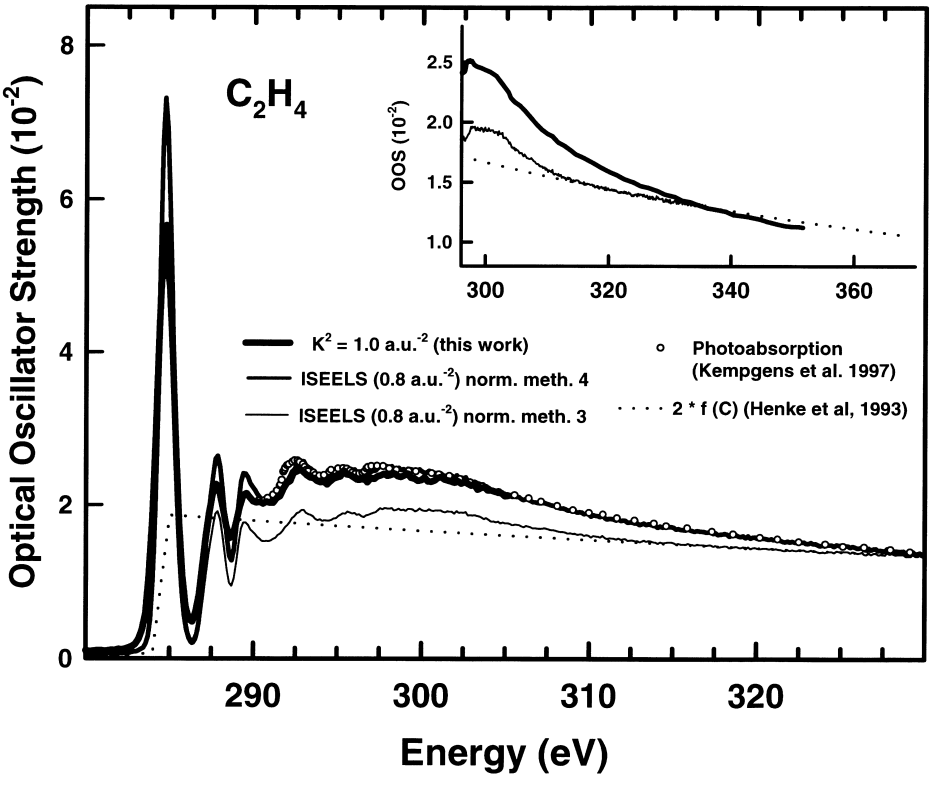

Fig. 6. Optical oscillator strength (OOS) spectrum of ethylene derived from low momentum transfer ISEELS. See caption to Fig. 3 for further details.

discrete region. Fig. 6 compares the optical spectrum derived from the ISEELS data using the two methods described above; first, by kinematic correction and matching to the experimental continuum values [32] (normalization method 4); second, by matching to the Henke atomic values [42] in the pre-edge and far-continuum regions (normalization method 3). In this case, there is quite a large difference between these two approaches. As with acetylene, at high energy, the continuum oscillator strength reported by Kempgens et al. [32] dips below the atomic value from the Henke table, as shown in the insert to Fig. 6. The experimental π* OOS from these approaches are summarized along with various computed values in Table 2. We have chosen the value obtained by matching to the experimental photoabsorption continuum (method 4) as that to use for conversion of relative to absolute GOS.

The GOS profiles for the π*, 3s and 3p features of ethylene are plotted in Fig. 7. As with acetylene, the curves are not structured, outside of our statistical errors, and the GOS profile for the 3s state is considerably less steep than those for the π* and 3p states, reflecting its relatively greater intensity at large scattering angle.

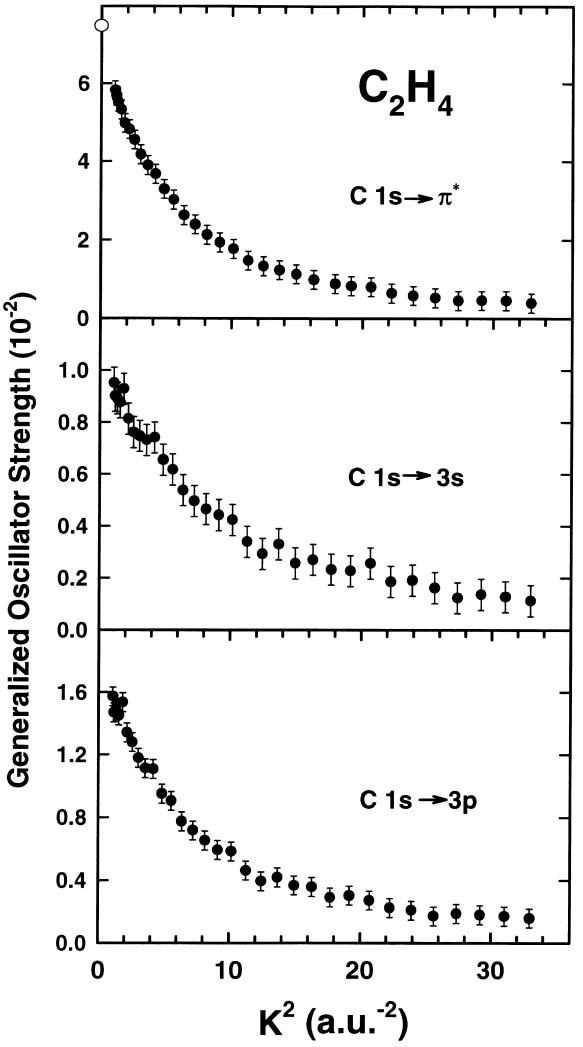

Fig. 7. Generalized oscillator strength profiles for π*, 3s and 3p C 1s excited states of ethylene. The absolute GOS scale was established by setting the extrapolated π* GOS at $K^2 = 0$ to an optical oscillator strength of 0.075, derived as outlined in the text.

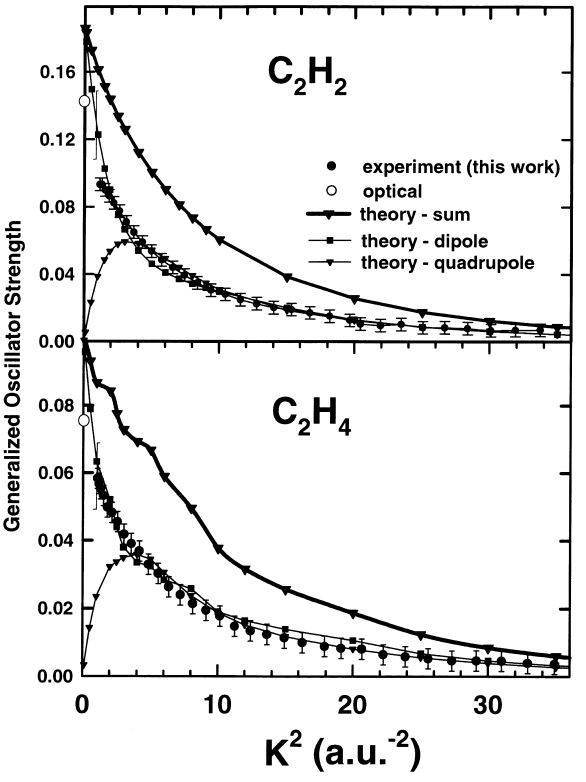

Fig. 8. Comparison of the experimental and calculated GOS profiles for the C 1s→π* transitions of acetylene and ethylene. The computed dipole, quadrupole and total GOS profiles are plotted. The large error bar indicates the range of possible absolute scales that could be consistent with the extrapolation of the relative GOS to $K^2 = 0$.

4.3. Comparison to theory

Relative to the present and previous [33] theoretical results, the optical oscillator strength (OOS) values for the C 1s→π* transitions derived from experiment are 28 and 25% lower, respectively, for acetylene and 41 and 30% for ethylene (Table 2). The rationale for the preferred experimentally-derived OOS values is explained above, based on the analysis presented in Figs. 3 and 6. Fig. 8 compares the absolute GOS profiles for the C 1s→π* transitions of acetylene and ethylene with those computed using ab-initio generalized multi structural wave functions. For each species, the computed total GOS includes strong contributions from the quadrupole C $1s\sigma_g \rightarrow \pi_g^*$ transition, except very close to $K = 0$. The shape and magnitude of the measured GOS profiles are in reasonable agreement with that computed for the dipole contribution alone. The experimental GOS profiles are also in good agreement with the shape of the total computed GOS profile outside of the low K^2 region. However, the magnitude of the experimentally-derived GOS profile is significantly lower than the computed total GOS profile for each species. Surprisingly, it is in quite good agreement with the dipole component over the whole momentum transfer range.

5. Discussion

At finite momentum transfer, the GOS profile consists of the sum of dipole, quadrupole and higher order electric multipole excitations (Eq. (2)) [26]. The contributions from the non-dipole terms become larger with higher momentum transfer due to the K^{2n} weighting factor. However, there will only be significant non-dipole contribution if there is an appreciable quadrupole matrix element. For both molecules, the main observation from the comparison of experiment and theory is that the experimental π* absolute GOS is a much better match to the dipole-only calculation than the sum of the computed dipole and quadrupole transitions. This was also found to be the case in the O 1s of CO_2 although in that work, because a small K^2 could not be reached on account of the much larger transition energy, the normalization to set the absolute GOS was carried out at finite momentum transfer.

The pronounced difference between the theoretical and experimental results may be explained by one or more of the following possibilities. First, the theoretical calculations may be overestimating the non-dipole contribution and, as consequence, the theoretical GOS profile is higher than the experimental one. We note that the theoretical calculations were carried out within the First Born Approximation (FBA) and higher order terms (non-FBA) may be contributing to the GOS, especially for larger values of the transferred momentum. The computed optical oscillator strength is considerably higher than all experimental estimates (Table 2). Non-vertical contributions [43] may be contributing preferentially to the non-dipole process. They were not considered in the present calculations, which were carried out at the ground state geometry only. Second, our procedure to estimate the OOS for the C 1s→π* transitions from the experimental results may be underestimating it. However the comparisons with literature optical values presented in Figs. 3 and 6 seem very sound. If the experimental OOS was higher, this would shift the experimental GOS to higher values, in better agreement with the computed total GOS. Further theoretical and experimental studies of the GOS of acetylene and ethylene are required to resolve the differences reported in this work.

Acknowledgements

Financial support for this research has been provided by FUJB and CNPq (Brazil), NSERC (Canada) and the Canada Research Chair program.

References

[1] C.E. Brion, Recent Advances in Electron Spectroscopy, MTP International, Rev. Phys. Chem. Ser. 1, Vol. 5. Butterworth, London, 1972, p. 55.
[2] W.C. Tam, C.E. Brion, J. Electron Spectrosc. Relat. Phenom. 2 (1973) 111.
[3] W.C. Tam, C.E. Brion, J. Electron Spectrosc. Relat. Phenom. 3 (1974) 269.
[4] W.C. Tam, C.E. Brion, J. Electron Spectrosc. Relat. Phenom. 3 (1974) 281.

[5] W.C. Tam, C.E. Brion, J. Electron Spectrosc. Relat. Phenom. 3 (1973) 479.
[6] W.C. Tam, C.E. Brion, J. Electron Spectrosc. Relat. Phenom. 4 (1974) 77.
[7] W.C. Tam, C.E. Brion, J. Electron Spectrosc. Relat. Phenom. 4 (1974) 139.
[8] W.C. Tam, C.E. Brion, J. Electron Spectrosc. Relat. Phenom. 4 (1974) 149.
[9] G.R. Wight, M.J. Van der Wiel, C.E. Brion, J. Phys. B 9 (1976) 675.
[10] A.P. Hitchcock, C.E. Brion, J. Electron Spectrosc. Relat. Phenom. 10 (1977) 317.
[11] C.E. Brion, S. Daviel, R.N.S. Sodhi, A.P. Hitchcock, AIP Conf. Proc. 94 (1982) 429.
[12] A.P. Hitchcock, D.C. Mancini, J. Electron Spectrosc. 67 (1994) 1, A 1998 update of this comprehensive bibliography of inner shell excitation studies of atoms and molecules is available from the corresponding author.
[13] J.T. Francis, C. Enkvist, S. Lunell, A.P. Hitchcock, Can. J. Phys. 72 (1994) 879.
[14] J.T. Francis, N. Kosugi, A.P. Hitchcock, J. Chem. Phys. 101 (1994) 10429.
[15] J.T. Francis, C.C. Turci, T. Tyliszczak, G.G.B. de Souza, N. Kosugi, A.P. Hitchcock, Phys. Rev. A 52 (1995) 4665.
[16] A.P. Hitchcock, I.G. Eustatiu, J.T. Francis, C.C. Turci, J. Electron Spectrosc. 88–91 (1998) 77.
[17] I.G. Eustatiu, T. Tyliszczak, A.P. Hitchcock, Chem. Phys. Lett. 300 (1999) 676.
[18] C.C. Turci, J.T. Francis, T. Tyliszczak, G.G.B. de Souza, A.P. Hitchcock, Phys. Rev. A 52 (1995) 4678.
[19] I.G. Eustatiu, J.T. Francis, T. Tyliszczak, C.C. Turci, A.L.D. Kilcoyne, A.P. Hitchcock, Chem. Phys. 257 (2000) 235.
[20] I.G. Eustatiu, T. Tyliszczak, A.P. Hitchcock, C.C. Turci, A.B. Rocha, C.E. Bielschowsky, Phys. Rev. A 61 (2000) 042505.
[21] T. Tyliszczak, I.G. Eustatiu, A.P. Hitchcock, C.C. Turci, A.B. Rocha, C.E. Bielschowsky, J. Electron Spectrosc. Relat. Phenom. 114–116 (2001) 93.
[22] A.P. Hitchcock, J. Electron Spectrosc. Relat. Phenom. 112 (2000) 9.
[23] E.N. Lassettre, A. Skerbele, Methods Exp. Phys. 3B (1974) 868.
[24] S. Trajmar, J.K. Rice, A. Kuppermann, in: L. Prigogine, S.A. Rice (Eds.), Adv. Chem. Phys, Vol. XVIII, Wiley, New York, 1970, p. 15;
R.A. Bonham, in: C.R. Brundle, A.D. Baker (Eds.), Electron Spectroscopy: Theory, Techniques and Applications, Vol. 3, Academic Press, New York, 1979, p. 127.
[25] H. Bethe, Ann. Phys. (Leipzig) 5 (1930) 325.
[26] M. Inokuti, Rev. Mod. Phys. 43 (1971) 297.
[27] M. Tronc, G.C. King, F.H. Read, J. Phys. B 12 (1979) 137.
[28] R. McLaren, S.A.C. Clark, I. Ishii, A.P. Hitchcock, Phys. Rev. A 36 (1987) 1683.
[29] B. Kempgens, A. Kivimaki, H.M. Köppe, M. Neeb, A.M. Bradshaw, J. Feldhaus, J. Chem. Phys. 107 (1997) 4219.
[30] A.L.D. Kilcoyne, M. Schmidbauer, A. Koch, K.J. Randall, J. Feldhaus, J. Chem. Phys. 98 (1993) 6735.
[31] B. Kempgens, H.M. Köppe, A. Kivimaki, M. Neeb, K. Maier, U. Hergenhahn, A.M. Bradshaw, Surf. Sci. 425 (1999) L376.
[32] B. Kempgens, H.M. Köppe, A. Kivimäki, M. Neeb, K. Maier, U. Hergenhahn, A.M. Bradshaw, Phys. Rev. Lett. 79 (1997) 35.
[33] S. Iwata, N. Kosugi, O. Nomura, Jpn. J. Appl. Phys. 17 (1978) 105.
[34] A.J. Barth, R.J. Buenker, S.G. Peyerimhoff, W. Butscher, Chem. Phys. 46 (1980) 149.
[35] M.P. de Miranda, C.E. Bielschowsky, H.M. Boechat Roberty, G.G.B. de Souza, Phys. Rev. A 49 (1994) 2399.
[36] Quantar Technology Inc., Santa Cruz, CA 95060.
[37] J.T. Francis, Ph.D. thesis, McMaster University, 1995.
[38] C.E. Bielschowsky, M.A.C. Nascimento, E. Hollauer, Phys. Rev. A 45 (1992) 7942.
[39] M.P. de Miranda, C.E. Bielschowsky, J. Mol. Struct. (Theochem) 282 (1993) 71.
[40] R.E. Farren, J.A. Sheehey, P.W. Langhoff, Chem. Phys. Lett. 177 (1991) 307.
[41] B.S. Itchkawitz, B. Kempgens, H.M. Köppe, J. Feldhaus, A.M. Bradshaw, W.B. Peatman, Rev. Sci. Instrum. 66 (1994) 1531.
[42] B.L. Henke, E.M. Gullikson, J.C. Davis, At. Data Nucl. Data Tables 54 (1993) 181.
[43] A.B. Rocha, A.S. Pimentel, C.E. Bielschowsky, J. Phys. Chem. A 106 (2002) 181.